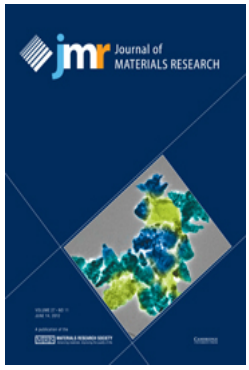

Electronic, magnetic and dielectric properties of multiferroic $MnTiO_3$

Xiaohui Deng, Wei Lu, Hai Wang, Haitao Huang and Jiyan Dai

Journal of Materials Research / Volume 27 / Issue 11 / 2012, pp 1421 - 1429
DOI: 10.1557/jmr.2012.101

Electronic, magnetic and dielectric properties of multiferroic $MnTiO_3$

Xiaohui Deng
Department of Physics and Electronic Information Science, Hengyang Normal University, Hengyang 421008, People's Republic of China

Wei Lu[a)]
Department of Applied Physics, The Hong Kong Polytechnic University, Hong Kong, People's Republic of China

Hai Wang
College of Materials Science and Engineering, Tongji University, Shanghai 201804, People's Republic of China

Haitao Huang and Jiyan Dai
Department of Applied Physics, The Hong Kong Polytechnic University, Hong Kong, People's Republic of China

(Received 5 January 2012; accepted 21 March 2012)

The ground-state structural, electronic, magnetic, optical and dielectric properties of $MnTiO_3$ are calculated using density functional theory within the generalized gradient approximation. The structure parameters obtained agree well with experimental results. The electronic structure results show that the G-type antiferromagnetic phase of LN-type $MnTiO_3$ has an indirect band gap of 0.85 eV. The calculated local magnetic moment of Mn ion is 4.19 μ_B. The calculated Born effective charges (BECs, denoted by tensor Z^*) show that the Z^* of Ti and O atoms are significantly and anomalously large. Interestingly, ferroelectric spontaneous polarization of large magnitude is predicted to be along [111] direction with a magnitude of 87.95–105.22 $\mu C/cm^2$. B-site Ti ions in 3 d^0 state dominate ferroelectric polarization of multiferroic $MnTiO_3$, whereas A-site Mn ions having partially filled 3 d^5 orbitals are considered to contribute to its antiferromagnetic properties. Furthermore, it is predicted that multiferroic $MnTiO_3$ shows good dielectric and optical properties.

I. INTRODUCTION

Perovskite-type (ABO_3) multiferroic materials have received considerable attention in recent years; the multiferroics have coupled magnetic, electric, and/or electronic structural order parameters that result in both (anti) ferromagnetism, ferroelectricity, and/or ferroelasticity in the same phase.[1–3] With this coexistence, they have the spontaneous magnetization that can be switched on by an applied magnetic field, also the spontaneous polarization that can be tuned by an electric field. Owing to the coupling between magnetic and ferroelectric orders, this can lead to magnetoeletric effect, in which magnetization can be switched on by an applied electric field and vice versa.[2–5] The mutual control of electric and magnetic properties is of significant interest for applications in memory storage devices, electric field-controlled ferromagnetic resonance devices, sensors, actuators and other potential devices.[6–9] Besides the application aspects of this technology, the fundamental physics of magnetoelectric coupling is also important for understanding the intrinsic physical properties. Many efforts have been devoted to theoretically investigate multiferroic materials over the last decade.[9–15] It is recognized that ferroelectricity and ferromagnetism are rarely found in the same system because the conventional off-center distortion of the B ion in d^0 state responsible for polar behavior is usually inconsistent with the partially filled d orbitals, which are a prerequisite for a magnetic ground state.

Fennie has proposed a strategy to design structures from symmetry principles, which stipulate that a polar lattice distortion induces weak ferromagnetism, and suggested that $LiNbO_3$ (LN)-type materials crystallizing in the high-pressure form with a magnetic ion such as $FeTiO_3$, $MnTiO_3$, and $NiTiO_3$, are candidates for multiferroic materials.[16] The prediction is thereafter validated by the synthesis of the high-pressure form of LN-type $FeTiO_3$ which is ferroelectric at and below room temperature and weakly ferromagnetic below 120 K.[17] Lately, Inaguma et al.[18] synthesized LN-type $MnTiO_3$ with space group *R*3c under high pressure and temperature. They investigated its properties and confirmed that this compound is also ferroelectric polar at room temperature and has weak ferromagnetism at 25 K. Recently, Shin et al.[19] experimentally demonstrated a high ferroelectric polarization level of ~47 $\mu C/cm^2$ in the heteroepitaxial thin film of LN-type $ZnSnO_3$ following its synthesis using high-pressure method.[20] For $MnTiO_3$, naturally, both

[a)]Address all correspondence to this author.
e-mail: ap17198@inet.polyu.edu.hk
DOI: 10.1557/jmr.2012.101

ferroelectric polarization and magnetic polarization, i.e., multiferroic properties, is also expected to exist in its high quality thin film. Magnetism should be controlled through an applied electric field as predicted by Fennie.[17] However, the detailed structural, electronic, magnetic and optical, as well as dielectric properties of LN-type $MnTiO_3$ have rarely been reported. Fundamental investigations are of importance for understanding the multiferroic materials as well as improving their practical applications.

In this work, we first present first-principles calculations on the structural stability for LN-type $MnTiO_3$ with different magnetic configurations. Then, the orbital hybridization and magnetic ordering as well as the origin of ferromagnetism and ferroelectricity are discussed. The remainder of this article is organized as follows. Using first-principles density functional theory (DFT) (Sec. II), we first study ground-state properties (Sec. III. A and III. B) such as the atomic and electronic structures with different magnetic configurations. Finally, we discuss dielectric properties (Sec. IV.A and Sec. IV.B) such as the BECs, the optical properties of multiferroic $MnTiO_3$.

II. COMPUTATIONAL METHOD

First-principles calculation, based on DFT, [21,22] is one of the most powerful tools to study the ground state property of materials. To calculate the electronic structure, BECs, spontaneous polarization and optical properties of LN-type $MnTiO_3$, we used generalized gradient approximation (GGA) proposed by Perdew et al.[23] as implemented in the Vienna ab initio Simulation Package (VASP).[24,25] All results are obtained using the projector-augmented plane-wave method (PAW).[26] Spin polarization was adopted when we performed magnetic calculations. The forces on the atoms are calculated using Hellmann-Feynman theorem and are used to perform structural relaxation using the conjugate gradient method. Structural optimizations were continued until the forces on the atoms had converged to less than 0.01 eV/Å. The final energies of the optimized geometries were recalculated so as to correct for changes in the plane-wave basis during relaxation. The self-consistent iteration was carried out with a total energy convergence tolerance of less than 0.01 meV. In the basis we included 7 valence electrons for Mn ($3d^6 4s^1$), 4 for Ti ($3d^3 4s^1$) and 6 for O ($2s^2 2p^4$). For total energy and electronic structure calculation, an energy cutoff of 440 eV was adopted and a $6 \times 6 \times 6$ Monkhorst–Pack[27] mesh was used for the ferroelectric $R3c$ and other $MnTiO_3$ structures considered in the present study. For linear response calculation, an energy cutoff of 500 eV was adopted and $8 \times 8 \times 8$ Monkhorst-pack k points were used. For optical property calculation,[28] an energy cutoff of 500 eV was adopted, 150 electron bands and $12 \times 2 \times 12$ Monkhorst-pack k-points were used.

III. GROUND STATE PROPERTIES

A. Structural and magnetic orders

The stable polymorph of $MnTiO_3$ at ambient conditions crystallizes in the ilmenite (IL) structure with space group $R\bar{3}$. At high temperatures and pressures, IL-type $MnTiO_3$ transforms to a denser $LiNbO_3$ -type phase through a cation reordering process.[18,29] Experimental results reveal that both IL-type and LN-type $MnTiO_3$ are antiferromagnetic (AFM).[18,30,31] As a comparison, the structural data of IL-type $MnTiO_3$ has also been calculated in this work. First, we determined the structural parameters of $MnTiO_3$ in its two phases by relaxing simultaneously both the cell shape and the atomic positions in G-type AFM order (where each magnetic atom is surrounded by six AFM neighbors). Both IL- and LN-type $MnTiO_3$ are rhombohedral with ten atoms in the unit cell. To describe their geometry, we use the primitive (rhombohedral) unit cell in this work. Atomic fractional positions are also given in rhombohedral coordinates. The calculated equilibrium structural parameters are given in Table I, where bulk modulus is determined by fitting the E–V (total energy versus volume) to Murnaghan's equation of state.[32] For comparison, the available experimental values are also given. The calculated volume agrees well with the experimental one. For LN-type $MnTiO_3$, the lattice parameter is overestimated by only 1.07%. The calculated lattice parameter combining with smaller calculated angle leads to a 1.9% overestimation along $<111>$. The negligible deviation between theoretical and experimental values indicates that GGA is satisfactory as a computational method to describe the structures of $MnTiO_3$.

To clarify which magnetic order is the ground state, we compared the total energies of LN-type $MnTiO_3$ in different magnetic configurations relative to the paramagnetic (PM) phase, which is a non spin-polarized case. The calculated total energy data are listed in Table II for the PM, ferromagnetic (FM) as well as G-type AFM state. As a comparison, the total energy of IL-type $MnTiO_3$ with FM and G-AFM configurations are also given. We find that the total energy of G-AFM is always lower than FM for both IL-type and LN-type phase. This means that AFM is more stable than FM one, being consistent with experimental reports.[30,31,18] It is also apparent that IL-type $MnTiO_3$ is stable than LN-type one, which is also consistent with the experiment.[29] Furthermore, we also built a $2 \times 2 \times 2$ supercell to create the two other possible AF arrangements, that is, A-type AFM and C-type AFM. In the A-AFM structure, each magnetic atom has two AFM and four FM for LN-type $MnTiO_3$, and one AFM and two FM for IL-type $MnTiO_3$ (vice versa in the case of C-AFM). The calculated total energies for A-AFM and C-AFM of LN-type and IL-type $MnTiO_3$ are slightly larger than G-type AFM, indicating that G-type AFM is the most stable state for both LN-type and IL-type $MnTiO_3$.

TABLE I. Optimized and experimental lattice parameters (a in Å, α in deg, and equilibrium volume V_0 in $Å^3$) atomic positions and bulk modulus (B_0 in GPa) of $MnTiO_3$ phase.

Phase	Unit cell parameters	Position	B (Gpa)
	a = 5.5250; α = 55.6606[a]	Ti (2a): 0, 0, 0 Mn (2a): 0.2857,0.2857,0.2857	155
	V_0 = 107.25	O (6b): 0.1078, 0.3648, 0.7179	
LN-type	a = 5.4667; α = 56.857[b]	Ti (2a): 0, 0, 0 Mn (2a): 0.2762,0.2762,0.2762	
	V_0 = 107.14	O (6b): 0.1235, 0.3460, 0.7207	
	a = 5.4657; α = 56.8803[c]	Ti (2a): 0, 0, 0 Mn (2a): 0.2760,0.2760,0.2760	
	V_0 = 107.15	O (6b): 0.1241, 0.3461, 0.7221	
	a = 5.5929; α = 54.5986[a]	Ti (2c): 0.1474,0.1474,0.1474 Mn (2c): 0.3566,0.3566,0.3566	161
	V_0 = 108.14	O (6f): 0.0503,0.4385,0.7744	
IL-type	a = 5.6095; α = 54.5125[d]		170[e]
	V_0 = 108.85		
	a = 5.6100; α = 54.5227[f]	Ti (2c) : 0.1444,0.1444,0.1444 Mn (2c) : 0.3609,0.3509,0.3509	
	V_0 = 108.91	O (6f): 0.0477,0.4395,0.7877	

[a]Present work.
[b]Reference 29.
[c]Reference 18.
[d,e]Reference 34, 42.
[f]Reference 43.

TABLE II. Total energy of various spin configurations of $MnTiO_3$ (relative to the LN-type PM in eV/f.u.).

	FM	G-AFM	A-AFM	C-AFM
LN-type	−0.7906	–0.8803	−0.8373	–0.8597
IL-type	−0.9996	–1.0725	−1.0351	–1.0588

B. Electronic and magnetic properties

Because LN-type $MnTiO_3$ has multiferroic properties, we will only present its electronic structure in three different magnetic order configurations.

For the non spin-polarization (i.e., PM) phase of LN-type $MnTiO_3$, the calculated partial density of states (PDOS) is shown in Fig. 1. Both PM- and FM phase are experimentally inaccessible phases, but provide a bridge to deeply understand the spin-polarized AFM electronic structure. The zero is set to the Fermi level. The lowest valence band (VB) starts around −19 eV originate from a filled and rather narrow O 2*s* orbitals, including also small contribution from Ti 3*d* electrons and very slight contribution from Ti 4*s*, Mn 4*s*, 3*d* electrons. Above these states, a broad band between −8 and −3 eV is mainly composed of O 2*p* states with small contribution from Ti 4*s*, 3*d* and Mn 4*s*, 3*d* states, which mean the presence of covalent bonding between Ti–O and Mn–O. The band at the Fermi level arises predominantly from the Mn 3*d* states with small Ti 3*d* and O 2*p* contribution. From the line shape analysis, we can see that the O and Ti are similar more than O and Mn, indicating that the hybridization between Ti–O is stronger than Mn–O. The large number of electrons near the Fermi level means that the PM phase is not a favorable condition for stability according to Stoner argument.[33] Lower energy structure could be expected by adopting spin polarization and structural distortion.

For FM phase of LN-type $MnTiO_3$, Fig. 2 shows the calculated band structure for both majority (solid line) and minority (dot line) spin states of along the high-symmetry directions in the Brillouin zone (BZ). The Fermi level is located at 0.0 eV. In the VB, the narrow energy band at the lowest region of −19 eV (not shown here) is formed mainly from O 2*s*, which is almost the same as PM phase. The energy range between −7 and −3 eV is mainly composed of O 2*p* states with small contribution from Ti 4*s*, 3*d* and Mn 4*s*, 3*d* states. The composition is same but the energy range is decreased compared with the PM phase. The band near the Fermi level splits into two parts compared with the same level in PM phase, which arises mainly from Mn 3*d* and small Ti 3*d* and O 2*p* contribution. The FM phase of LN-type $MnTiO_3$ has an insulator character with a band gap of 0.76 eV (GGA). The band gap is indirect, with the bottom of the conduction band (CB) located between G and F in the primitive Brillouin zone and the top of the VB at the point F. The calculated local magnetic moments are 0.29 μ_B, 4.32 μ_B and 0.05 μ_B for Ti, Mn, O, respectively. The total magnetic moment (including those at Ti, O and interstitial sites) is 5 μ_B/f.u. This value is smaller than the reported effective Bohr magneton number (5.85).[18] According to previous theoretical investigation on $BiFeO_3$, [local spin density approximation (LSDA)] (GGA) +U method improves the agreement with experimental values for magnetic moment.[13,35] The magnetic moment of Mn reduced from the formal value of 5 μ_B for high spin Mn^{2+}. The non-integer magnetic moment at Mn sites and slight increment of local magnetic moments of Ti and O are contributed to the hybridization Ti–O and Mn–O.

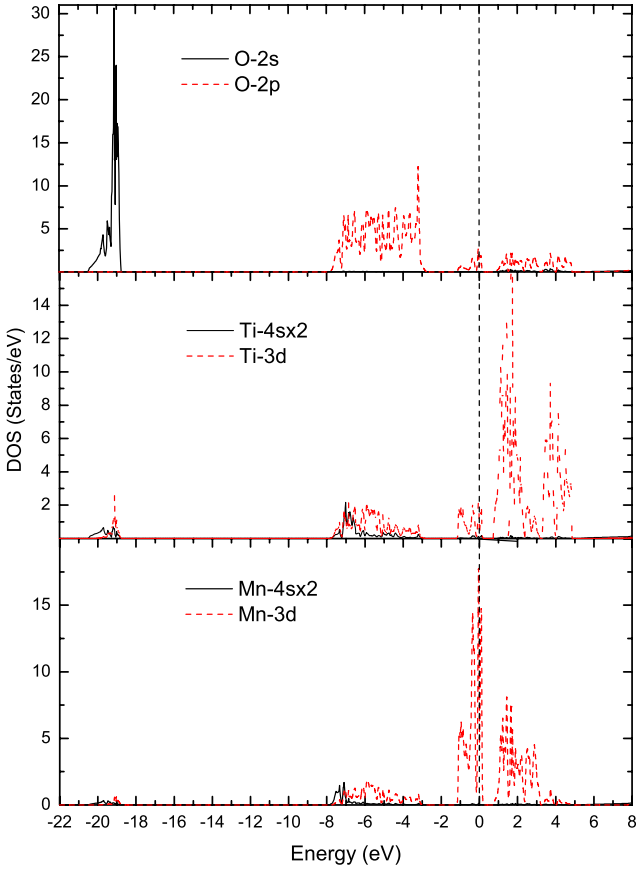

FIG. 1. Partial density of states of paramagnetic LN-type $MnTiO_3$ phase. Fermi energy is set to zero.

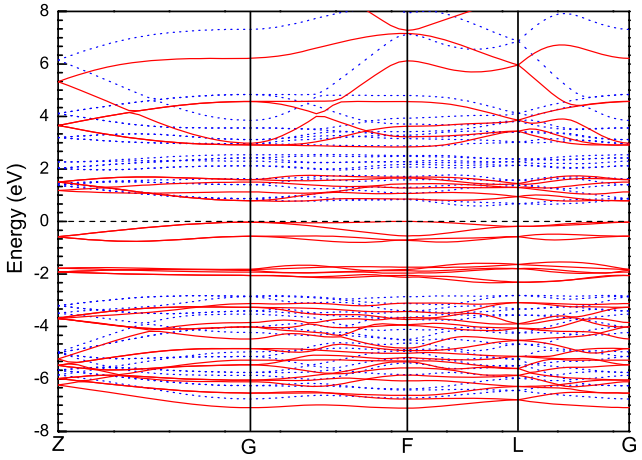

FIG. 2. Electronic band structure for majority (solid line) and minority (dot line) spin states of ferromagnetic LN-type $MnTiO_3$ phase along the high-symmetry directions in the Brillouin zone. The Fermi level is located at 0.0 eV.

The total DOS of LN-type $MnTiO_3$, calculated with G-AFM magnetic order, is shown for both spin channels in Fig. 3(a), along with the partial DOS of O, Ti and Mn [Figs. 3(b)–3(d)]. Due to the antiferromagnetic nature, all

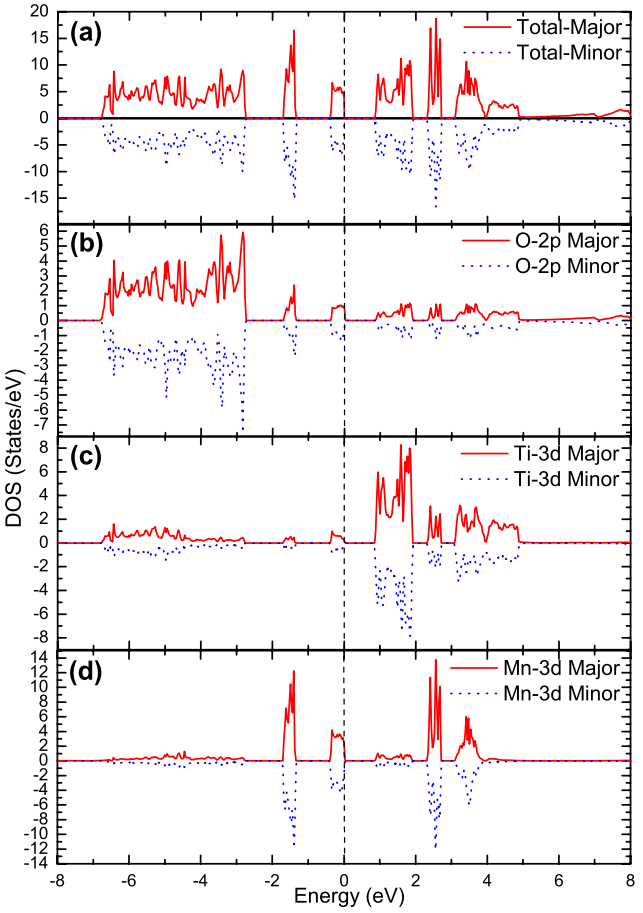

FIG. 3. Total electronic DOS (a) and the partial DOS of O 2*p* (b), Ti 3*d* (c), and Mn 3*d* (d) of G-antiferromagnetic LN-type $MnTiO_3$, respectively. Majority and minority spins are shown above and below the axes, respectively. Fermi energy is set to zero.

the major spin in the total and partial DOS are almost equal to the minor spin. It can be seen that VB is mainly composed of three energy bands. They are between −7 and −3 eV, around −1.5 eV and near Fermi level. By comparing analysis of Figs. 3(b)–3(d) and Fig. 2, we find that the contribution of the three parts is almost same, but the energy gaps are increased between two of them. The electrons in G-AFM phase display more localization compared with FM, suggesting that G-AFM is more stable. This is consistent with the result for the total energy. The band gap of 0.85 eV is slightly increased compared with FM phase. According to the band structure analysis, it is also an indirect gap with the bottom of the CB located between L and G in the primitive Brillouin zone and the top of the VB at the point L in the supporting information). At present, we don't get any valuable experimental report for comparison. It is worth noting that the density function calculations are known to underestimate the band gap and hence the reported values will be lower than the real band-gap value. To get the best description of the electronic structure of LN-type $MnTiO_3$,

photoemission spectroscopy will be useful experimental data. The calculated local magnetic moment of Mn ion is 4.19 μ_B. As we discussed in the above paragraph, the GGA +U method can improve the agreement with the experimental value for magnetic moment. For the optimized G-AFM LN-type $MnTiO_3$, the bond distance between Ti and O are 2.138 and 1.900 Å meanwhile the bond lengths of Mn-O are 2.215 and 2.068 Å. The shorter bond length indicates a stronger hybridization of Ti–O than Mn–O. Since the hybridization of Ti–O is stronger than Mn–O, the Ti ion in the B site in d^0 state will dominate the polar behavior, meanwhile the Mn ion in the A site with the partially filled $3d^5$ orbitals is responsible for antiferromagnetic ground state. This should be the reason why LN-type A (Mn, Fe, Ni) TiO_3 can be a potential material as multiferroic.

IV. DIELECTRIC PROPERTIES

A. Born effective charges and Ferroelectric polarization

In this subsection, we present the BECs of $MnTiO_3$ computed for both ferroelectric $R3c$ and paraelectric $R\bar{3}c$ phases. One should note that $LiNbO_3$ has two phases with trigonal symmetry: a high symmetric paraelectric phase with space group $R\bar{3}c$ stable above 1480 K and a ferroelectric ground state with space group $R3c$.[36] According to previous reports,[9,13,37] the $R\bar{3}c$ phase is always selected as a paraelectric structure for theoretical investigation of LN-type ABO_3 ferroelectric properties. By analogy to $LiNbO_3$ and other isostructures, $R\bar{3}c$ structure is a possible candidate for high-temperature paraelectric phase of LN-type $MnTiO_3$. By comparing analyses of the Wyckoff positions of space group $R\bar{3}c$ and $R\bar{3}c$, we can conclude that the sites of (2a) Ti (0, 0, 0), (2a) Mn (0.2857, 0.2857, 0.2857) in $R3c$ structure will transform to the sites of (2b) Ti (0, 0, 0), (2a) Mn (1/4, 1/4, 1/4) in $R\bar{3}c$ structure, respectively. The site of (6b) O (0.1078, 0.3648, 0.7179) in $R\bar{3}c$ structure will be selected as a reference of the initial site of (6e) O (−x, x + 1/2, 3/4) (where −x = 0.1078) in $R\bar{3}c$ structure for optimization. The lattice parameters of the ferroelectric phase are taken as the initial values. The structural parameters of the paraelectric phase, relaxed simultaneously the cell shape and the atomic positions with G-type AFM order, are listed in Table III.

TABLE III. Optimized lattice parameters (a in Å, α in deg, and equilibrium volume V_0 in $Å^3$) atomic positions for antiferromagnetic $MnTiO_3$ in the ferroelectric $R3c$ and paraelectric $R\bar{3}c$ phase.

Phase	Unit cell parameters	Position
	a = 5.5250;	Ti (2a): 0, 0, 0 Mn (2a):
	α = 55.6606	0.2857,0.2857,0.2857
Ferroelectric	V_0 = 107.25	O (6b): 0.1078, 0.3648, 0.7179
Paraelectric	a = 5.4189;	Ti (2b): 0, 0, 0 Mn (2a):
	α = 57.1892	0.25,0.25,0.25
	V_0 = 105.23	O (6e): 0.1319, 0.3681, 0.75

BECs (Z^*), defined by the change in polarization created by atomic displacement, are a fundamental quantity for the study of insulating crystal lattice dynamics. The BECs control the long-range Coulomb interaction between the nuclei, thus BEC is important in terms of the theoretical study of ferroelectrics since the ferroelectric transition takes place due to the opposing effects of long-range Coulomb interactions and short-range repulsions. The Born effective charges tensors $Z^*_{\kappa,\alpha\beta}$ can be expressed as a linear term of polarization per unit cell in direction β induced by displacement of ion κ in direction α without macroscopic electric field effect or the force exerted on the atom by an electric field in the direction β,

$$Z^*_{k,\alpha\beta} = \frac{\Omega_0}{|e|}\frac{\partial P_\beta}{\partial u_{\kappa,\alpha}}\bigg|_{\varepsilon=0} = \frac{\Omega_0}{|e|}\frac{\partial F_{\kappa,\alpha}}{\partial E_\beta} \quad . \qquad (1)$$

To calculate the BECs, we use density functional perturbation theory (DFPT)[38] of the linear response formalism. Table IV summarizes the results of BECs for Ti, Mn, and three oxygen atoms. The tensors are reported in Cartesian coordinates with the z-axis along the [111] primitive cell direction (x perpendicular to **b** axis, y along **b** axis and z along **c** axis in hexagonal cell). It shows that Z^* of Ti and Mn is nearly isotropic and the value along z-axis is slightly different from that along x- and y-axis. For the O, the BECs tensor exhibits strong anisotropic character with the presence of finite off-diagonal elements as well. It is known that the formal valence of Ti, Mn and O in $MnTiO_3$ are +4, +2 and −2, respectively. Since Z^* can reflect the covalency of the bonding environment of each atom with respect to their formal valence, comparing these values with Z^* in these two structures, we find that the Z^* of Ti and O atoms are significantly anomalously large. The maximum changes for Ti and O are +88.8% and −111.5% compared with the nominal charge expected in a purely ionic crystal, revealing that a large dynamic contribution superimposed to the static charge, that is, a strong covalence effect. This anomalism as an important feature commonly also was found in other ferroelectric compounds.[9,36,39] The maximum change for Mn is only +23.5% compared with the static charge, indicating a relative smaller covalence effect than Ti. This is consistent with our conclusion deduced from DOS and bond length calculated above. By comparing analysis of the Z^* of Ti and O in the two different structures, it can be seen that the absolute value of $Z^*_{ii\ (i = x\sim z)}$ in $R\bar{3}c$ phase is larger than that in $R3c$ phase whereas the value change of Mn is slight.

Spontaneous polarization ($\mathbf{P}_s$) is one of the basic quantities of ferroelectrics, which can be calculated from the difference between the polarization of a ferroelectric

phase and paraelectric phase. If Eq. (1) is approximately expressed by a finite difference expression, the $\mathbf{P_s}$ can be estimated by the following equation:

$$P_{s,\alpha} \cong \frac{|e|}{\Omega_0} \sum_{\kappa,\beta} Z^*_{\kappa,\alpha\beta} \Delta u_{\kappa,\beta} \quad , \qquad (2)$$

where $\Delta u_{\kappa,\beta}$ is the displacement of ion κ in Cartesian direction β. Assuming that a continuous adiabatic transformation takes place from paraelectric to ferroelectric phase and zero polarization in paraelectric phase because of absence of dipole, the spontaneous polarization can be obtained by keeping the optimized paraelectric phase lattice parameter and changing the atomic position from paraelectric phase to ferroelectric phase. The calculated results are listed in Table V. It can be seen that the polarization values are very much direction-dependent. The polarization values along x- and y-axis are very small, about zero. The spontaneous polarization is mainly along [111] (z-axis) direction with a value 87.95 μC/cm^2 and 105.22 μC/cm^2 by using $Z^*_{ij(i,j\ =\ x\sim z)}$ of ferroelectric and paraelectric phase, respectively. Our calculated results show that the spontaneous polarization value of LN-type $MnTiO_3$ ferroelectric phase is comparable with that of $LiNbO_3$[36] and multiferroic $BiFeO_3$.[2,9,13] Our result is consistent with the reported value by Fennie[16] using modern theory of polarization within LSDA + U framework.

TABLE IV. Born effective charges tensor for antiferromagnetic $MnTiO_3$ in the ferroelectric *R*3c and paraelectric *R*$\bar{3}$c phase.

	Ferroelectric phase			Paraelectric phase		
	6.47	0.63	0.00	7.52	0.89	0.00
Ti	−0.63	6.47	0.00	−0.89	7.52	0.00
	0.00	0.00	5.09	0.00	0.00	7.55
	2.47	0.11	0.00	2.42	0.00	0.00
Mn	−0.11	2.47	0.00	0.00	2.42	0.00
	0.00	0.00	2.29	0.00	0.00	2.33
	−2.11	−0.37	−0.09	−2.86	−0.79	−0.84
O1	−0.97	3.85	−1.44	−0.79	−3.77	−1.46
	−0.38	−0.99	−2.46	−0.97	−1.68	−3.29
	−4.00	−0.12	1.29	−4.23	0.00	1.69
O2	−0.72	−1.96	0.64	0.00	−2.40	0.00
	1.04	0.17	−2.46	1.94	0.00	−3.29
	−2.84	1.39	−1.20	−2.85	0.79	−0.84
O3	0.79	−3.13	0.80	0.79	−3.77	1.46
	−0.67	0.82	−2.46	−0.97	1.68	−3.29

TABLE V. Spontaneous polarization components (μC/cm^2) in Cartesian coordinate of ferroelectric $MnTiO_3$ obtained from Eq. (2) along a pathway from paraelectric phase to ferroelectric phase by using the Born effective charges ($Z^*_{ij(i,j=x\sim z)}$) of ferroelectric and paraelectric phase, respectively.

$Z^*_{ij(i,j=x\sim z)}$	P_x	P_y	P_z
Ferroelectric	0.00	0.03	87.95
Paraelectric	−0.06	0.00	105.22

B. Optical properties

The static and frequency-dependent dielectric response functions, such as absorption, refractive index or extinction coefficient, are important for the interpretation of the optical properties measured in the experiment. In this subsection, we investigate the dielectric and optical properties of LN-type $MnTiO_3$ with G-AFM magnetic order. It is known that the dielectric function is mainly connected with the electronic response. The imaginary part of the dielectric function $\varepsilon_2(\omega)$ was determined from the momentum matrix elements between the occupied and unoccupied wave functions,[28]

$$\varepsilon_2^{\alpha,\beta}(\omega) = \frac{4\pi^2 e^2}{\Omega_0} \lim_{q\to 0} \frac{1}{q^2} \sum_{c,v,\mathrm{K}} 2w_{\mathrm{K}} \delta(\varepsilon_{c\mathrm{K}} - \varepsilon_{v\mathrm{K}} - \omega) \times \langle u_{c\mathrm{K}+e_\alpha q} \mid u_{v\mathrm{K}} \rangle \langle u_{c\mathrm{K}+e_\beta q} \mid u_{v\mathrm{K}} \rangle^* \quad , \qquad (3)$$

where Ω_0 is the unit-cell volume, ω is the photon energy, c and *v* refer to conduction and valence band states respectively, the vectors e_α are unit vectors for the three Cartesian directions, and $u_{\mathbf{ck}}$ is the cell periodic part of the wave functions at the k-point **k**. The real part of the dielectric function $\varepsilon_1(\omega)$ is obtained by the usual Kramers-Kronig transformation. Optical constants, such as, the energy dependence of absorption coefficient α (ω), the refractive index n (ω), extinction coefficient κ (ω), energy-loss spectrum L (ω), as well as reflectivity R (ω) can be derived from the following expressions:

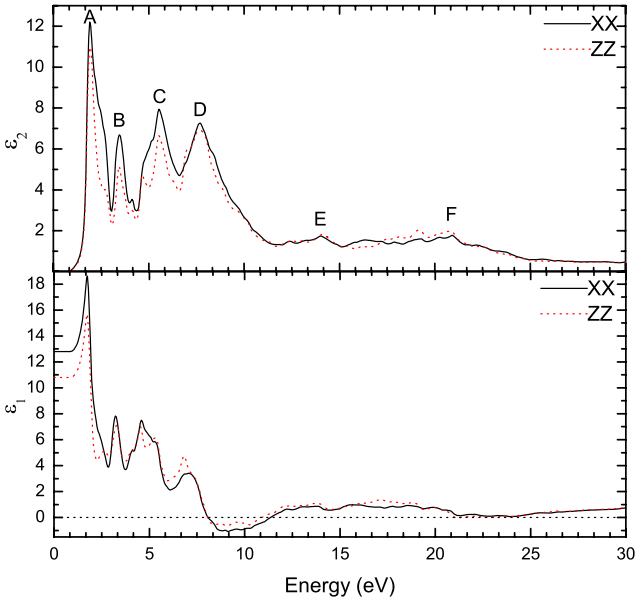

FIG. 4. The imaginary part $\varepsilon_2(\omega)$ and real part $\varepsilon_1(\omega)$ of the dielectric function of LN-type $MnTiO_3$. The solid and dot lines represent the polarization direction of xx and zz, respectively.

$$\alpha(\omega) = \omega \times \sqrt{2 \times (\sqrt{\varepsilon_1^2(\omega) + \varepsilon_2^2(\omega)} - \varepsilon_1(\omega))} \quad . \quad (4)$$

$$n(\omega) = \sqrt{\frac{\sqrt{\varepsilon_1^2(\omega) + \varepsilon_2^2(\omega)} + \varepsilon_1(\omega)}{2}} \quad , \quad (5)$$

$$k(\omega) = \sqrt{\frac{\sqrt{\varepsilon_1^2(\omega) + \varepsilon_2^2(\omega)} - \varepsilon_1(\omega)}{2}} \quad , \quad (6)$$

$$L(\omega) = \frac{\varepsilon_2(\omega)}{\varepsilon_1^2(\omega) + \varepsilon_2^2(\omega)} \quad , \quad (7)$$

$$R(\omega) = \left| \frac{\sqrt{\varepsilon(\omega)} - 1}{\sqrt{\varepsilon(\omega)} + 1} \right|^2 \quad , \quad (8)$$

where $\varepsilon(\omega) = \varepsilon_1(\omega) + i\varepsilon_2(\omega)$ is the complex dielectric function.

The calculated dielectric functions are displayed in Fig. 4, where the solid and dot lines represent the results along the direction of xx and zz, respectively. The imaginary and real parts exhibit an anisotropic character a lower energy range (about below 8 eV). The calculated optical dielectric permittivity tensors without local field effect are $\varepsilon_{XX}^{\infty} = \varepsilon_{YY}^{\infty} = 12.80$, $\varepsilon_{ZZ}^{\infty} = 10.80$. When local field effect is taken into consideration, the ion-clamped static dielectric tensors are $\varepsilon_{XX}^{\infty} = \varepsilon_{YY}^{\infty} = 12.61$, $\varepsilon_{ZZ}^{\infty} = 10.13$. The imaginary part $\varepsilon_2(\omega)$ of the dielectric function is directly connected with the energy band structure of G-AFM LN-type ferroelectric $MnTiO_3$ phase. There are mainly six peaks in the imaginary part of the dielectric function. The first peak A at about 1.94 eV corresponds mainly to the transition from O 2*p* VB near Fermi level to Ti 3*d* CB. The peaks B (3.45 eV), C (5.54 eV), and D (7.66 eV) are due to the transition from O 2*p* VB to Ti 3*d* and Mn 3*d* CB. Peak E (about 14.05 eV) is ascribed to the transition of inner electrons from Ti 4*s* or O 2*p* levels to CB. Peak F (20.90 eV) corresponds mainly to the excitation of inner electrons from VB state O 2*s* level to CB. It is worth

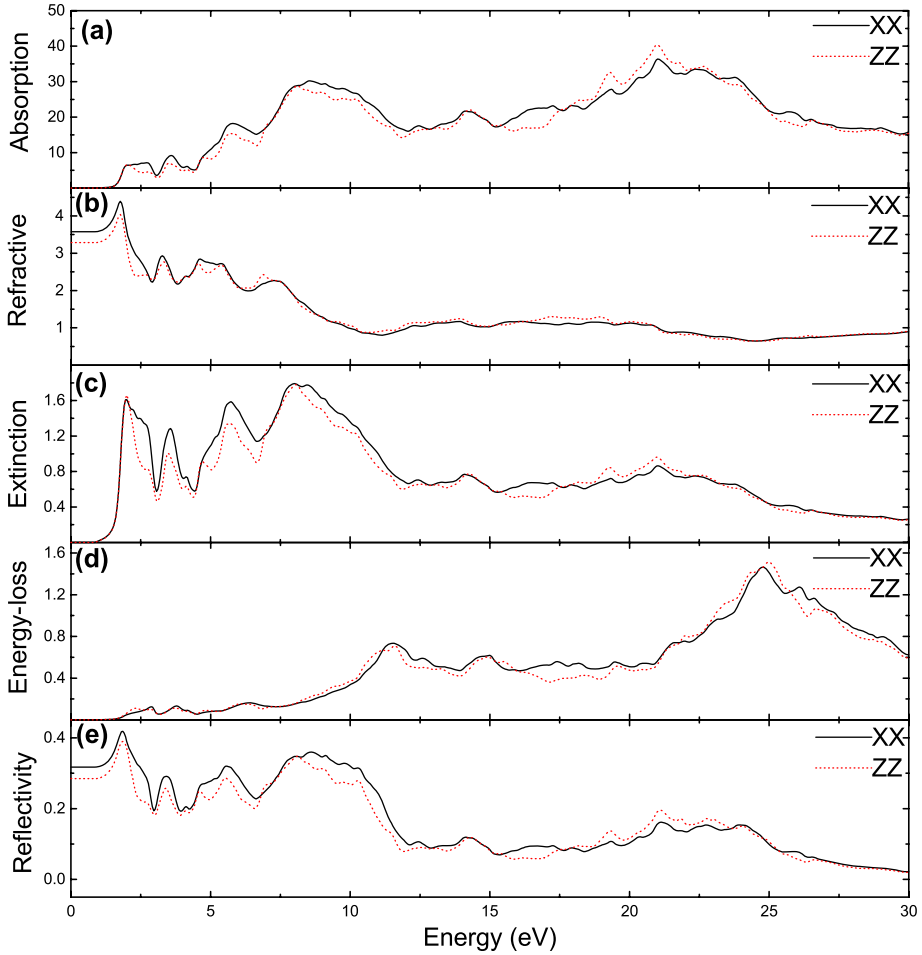

FIG. 5. The calculated optical constants of the ferroelectric $MnTiO_3$ phase (a) absorption spectrum, (b) refractive index, (c) extinction coefficient, (d) energy-loss spectrum, and (e) reflectivity along the direction of xx and zz, respectively.

noting that a peak in ε_2 (ω) does not correspond to a single interband transition since many direct or indirect transitions may be found in the band structure with an energy corresponding to the same peak.[40]

Figures 5(a)–5(e) show the calculated results on the energy dependence of absorption coefficient, refractive index, extinction coefficient, energy-loss spectrum, and reflectivity, respectively. The absorption spectrum is very large and decreases rapidly in the low-energy region. The refractive index shows an anisotropic character in the energy range from 0 to 8 eV accompanied by a change of the sign of birefringence $\Delta n = n_{zz}–n_{xx}$ from negative to positive. The reflectivity is lower than 32% for energy range from 0 to 1.1 eV along x-axis and 0 to 1.5 eV along z-axis, which indicates that photons penetrate through LN-type $MnTiO_3$ easier along z-axis than along x-axis. LN-type $MnTiO_3$ is transparent for photons with energy less than 1.5 eV along z-axis. Interestingly the reflectivity is lower than 15% in the range of 12–20 eV, suggesting potential application using these high-energy photons. The large extinction coefficient is consistent with reflectivity in the range of 1.5–11 eV. The energy-loss spectrum is related to the energy loss of a fast electron traversing in the material. The peak of the calculated loss spectrum is at about 11.5 and 24.8 eV, which is associated with the plasma oscillation.[41] This corresponds to a rapid decrease of reflectance in Fig. 5(e). This process is associated with transitions from the occupied O 2*s*, Ti 4*s* and O 2*p* bands, lying below the VB, to an empty CB.

V. CONCLUSION

Using the projector-augmented plane-wave potential approach to DFT within the GGA, we studied the structural, electronic, magnetic and dielectric properties of multiferroic LN-type $MnTiO_3$ phase. The fully relaxed structural parameters are in good agreement with the experimental data. We found that G-type AFM is the most stable magnetic order state in energy for both LN-type and IL-type $MnTiO_3$ phase. The electronic structures of G-AFM LN-type $MnTiO_3$ reveal that it has an indirect band gap of 0.85 eV. The calculated local magnetic moment of Mn ion is 4.19 μ_B. The hybridization of Ti–O is stronger than that of Mn–O, the Ti ion in the B site in d^0 state will dominate the polar behavior, meanwhile the Mn ion in the A site with the partially filled 3 d^5 orbitals is responsible for antiferromagnetic ground state, which play important roles for LN-type $MnTiO_3$ as potential multiferroic material.

The analysis of the Born effective charges showed that the Z^* of Ti and O atoms are significantly anomalously larger than their nominal ionic charge, whereas the Z^* of Mn does not change so much. The maximum changes for Mn, Ti, and O are +23.5%, +88.8%, and −111.5%, respectively, compared with the nominal charge expected in a purely ionic crystal. We also found that the absolute value of $Z^*_{ii\ (i = x\sim z)}$ in $R\bar{3}c$ phase is larger than that in $R3c$ phase; whereas the value of Mn almost unchanged. All of these results were originated from the fact that Ti–O has a strong covalence effect, meanwhile a smaller covalence effect between Mn–O. Under a finite difference expression approximation, the calculated spontaneous polarization is mainly along [111] (z-axis) direction with a value 87.95–105.22 $\mu C/cm^2$.

The calculated dielectric functions revealed that the imaginary and real parts exhibit an anisotropic character at lower energy range. The ion-clamped static dielectric tensors are $\varepsilon^{\infty}_{XX} = \varepsilon^{\infty}_{YY} = 12.61$, $\varepsilon^{\infty}_{ZZ} = 10.13$ with local field effect. According to the complex dielectric functions, other optical constants such as absorption spectrum, refractive index, extinction coefficient, energy-loss spectrum, and reflectivity were obtained and discussed in detail.

ACKNOWLEDGMENTS

This work was supported by the Hong Kong Polytechnic University (Project: A-PK26) and the National Science Foundation of China (No. 10902029).

REFERENCES

1. E.K.H. Salje: *Phase Transitions in Ferroelectic and Coelastic Crystal* (Cambridge University Press, Cambridge, UK, 1990).
2. J. Wang, J.B. Neaton, H. Zheng, V. Nagarajan, S.B. Ogale, B. Liu, D. Viehland, V. Vaithyanathan, D.G. Schlom, U.V. Waghmare, N.A. Spaldin, K.M. Rabe, M. Wuttig, and R. Ramesh: Epitaxial $BiFeO_3$ multiferroic thin film heterostructures. *Science* **299**, 1719–1722, 2003.
3. M. Fiebig, T.H. Lottermoser, D. Fröhlich, A.V. Goltsev, and R.V. Pisarev: Observation of coupled magnetic and electric domains. *Nature* **419**, 818, 2002.
4. T. Lottermoser and M. Fiebig: Magnetoelectric behavior of domain walls in multiferroic $HoMnO_3$. *Phys. Rev. B* **70**, 220407, 2004.
5. T. Kimural, T. Goto, H. Shintani, K. Ishizaka, T. Arima, and Y. Tokura: Magnetic control of ferroelectric polarization. *Nature* **426**, 55, 2003.
6. K. Taniguchi, N. Abe, S. Ohtani, and T. Arima: Magnetoelectric memory effect of the nonpolar phase with collinear spin structure in multiferroic $MnWO_4$. *Phys. Rev. Lett.* **102**, 147201, 2009.
7. J. Dho, X.D. Qi, H. Kim, J.L. MacManus-Driscol, and M.G. Blamire: Large electric polarization and exchange bias in multiferroic $BiFeO_3$. *Adv. Mater.* **18**, 1445, 2006.
8. Y.H. Chu, L.W. Martin, M.B. Holcomb, M. Gajek, S.J. Han, Q. He, N. Balke, H.H. Yang, D. Lee, W. Hu, Q. Zhan, P.L. Yang, A. Fraile-Rodríguez, A. Scholl, S.X. Wang, and R. Ramesh: Electric-field control of local ferromagnetism using a magnetoelectric multiferroic. *Nat. Mater.* **7**, 478, 2008.
9. P. Ravindran, R. Vidya, A. Kjekshus, H. Fjellvåg, and O. ErikssonPhys: Theoretical investigation of magnetoelectric behavior in $BiFeO_3$. *Phys. Rev. B* **74**, 224412, 2006.
10. N.A. Hill: Why are there so few magnetic ferroelectrics? *J. Phys. Chem. B* **104**, 6694, 2000.

11. R. Seshadri and N.A. Hill: Visualizing the role of Bi 6s "Lone Pairs" in the off-center distortion in ferromagnetic $BiMnO_3$. *Chem. Mater.* **13**, 2892, 2001.
12. N. Lampis, C. Franchini, G. Satta, A. Geddo-Lehmann, and S. Massidda: Electronic structure of $PbFe_{1/2}Ta_{1/2}O_3$: Crystallographic ordering and magnetic properties. *Phys. Rev. B* **69**, 064412, 2004.
13. J.B. Neaton, C. Ederer, U.V. Waghmare, N.A. Spaldin, and K.M. Rabe: First-principles study of spontaneous polarization in multiferroic $BiFeO_3$. *Phys. Rev. B* **71**, 014113, 2005.
14. B.B. Van Aken, T.T.M. Palstra, A. Filippetti, and N.A. Spaldin: The origin of ferroelectricity in magnetoelectric $YMnO_3$. *Nat. Mater.* **3**, 164, 2004.
15. M.Q. Cai, J.C. Liu, G.W. Yang, Y.L. Cao, X. Tan, X.Y. Chen, Y.G. Wang, L.L. Wang, and W.Y. Hu: First-principles study of structural, electronic, and multiferroic properties in $BiCoO_3$. *J. Chem. Phys.* **126**, 154708, 2007.
16. C.J. Fennie: Ferroelectrically induced weak ferromagnetism by design. *Phys. Rev. Lett.* **100**, 167203, 2008.
17. T. Varga, A. Kumar, E. Vlahos, S. Denev, M. Park, S. Hong, T. Sanehira, Y. Wang, C.J. Fennie, S.K. Streiffer, X. Ke, P. Schiffer, V. Gopalan, and J.F. Mitchell: Coexistence of weak ferromagnetism and ferroelectricity in the high-pressure $LiNbO_3$-type phase of $FeTiO_3$. *Phys. Rev. Lett.* **103**, 047601, 2009.
18. A. Aimi, T. Katsumata, D. Mori, D. Fu, M. Itoh, T. Kyômen, K. Hiraki, T. Takahashi, and Y. Inaguma: High-pressure synthesis and correlation between structure, magnetic, and dielectric properties in $LiNbO_3$-type $MnMO_3$ (M = Ti, Sn). *Inorg. Chem.* **50**, 6392, 2011.
19. J.Y. Son, G. Lee, M. Jo, H. Kim, H.M. Jang, and Y. Shin: Heteroepitaxial ferroelectric $ZnSnO_3$ thin film. *J. Am. Chem. Soc.* **131**, 8386, 2009.
20. Y. Inaguma, M. Yoshida, and T. Katsumata: A polar oxide $ZnSnO_3$ with a $LiNbO_3$-type structure. *J. Am. Chem. Soc.* **130**, 6704, 2008.
21. P. Hohenberg and W. Kohn: Inhomogeneous electron gas. *Phys. Rev.* **136**, B864, 1964.
22. W. Kohn and L.J. Sham: Self-consistent equations including exchange and correlation effects. *Phys. Rev.* **140**, A1133, 1965.
23. J.P. Perdew, K. Burke, and M. Ernzerhof: Generalized gradient approximation made simple. *Phys. Rev. Lett.* **77**, 3865, 1996.
24. G. Kresse and J. Hafner: Ab initio molecular dynamics for liquid metals. *Phys. Rev. B* **47**, 558, 1993.
25. G. Kresse and J. Furthmüller: Efficient iterative schemes for ab initio total-energy calculations using a plane-wave basis set. *Phys. Rev. B* **54**, 11169, 1996.
26. P.E. Blöchl: Projector augmented-wave method. *Phys. Rev. B* **50**, 17953, 1994.
27. H.J. Monkhorst and J.D. Pack: Special points for Brillouin-zone integrations. *Phys. Rev. B* **13**, 5188, 1976.
28. M. Gajdoš, K. Hummer, G. Kresse, J. Furthmüller, and F. Bechstedt: Linear optical properties in the projector-augmented wave methodology. *Phys. Rev. B* **73**, 045112, 2006.
29. J. Ko and C.T. Prewitt: High-pressure phase transition in $MnTiO_3$ from the ilmenite to the $LiNbO_3$ structure. *Phys. Chem. Miner.* **15**, 355, 1988.
30. P.B. Fabritchnyi, M.V. Korolenko, M.I. Afanasov, M. Danot, and E. Janod: Mössbauer characterization of tin dopant ions in the antiferromagnetic ilmenite $MnTiO_3$. *Solid State Commun.* **125**, 341, 2003.
31. N. Mufti, G.R. Blake, M. Mostovoy, S. Riyadi, A.A. Nugroho, and T.T.M. Palstra: Magnetoelectric coupling in $MnTiO_3$. *Phys. Rev. B* **83**, 104416, 2011.
32. F.D. Murnaghan: Finite deformations of an elastic solid. *Am. J. Math.* **49**, 235, 1937.
33. E.C. Stoner: Collective Electron Ferromagnetism. *Proc. R. Soc. London, Ser. A* **165**, 372, 1938.
34. N.L. Ross, J. Ko, and C.T. Prewitt: A new phase transition in $MnTiO_3$: $LiNbO_3$-perovskite structure. *Phys. Chem. Miner.* **16**, 621, 1989.
35. H. Wang, Y. Zheng, M.Q. Cai, H.T. Huang, and H.L.W. Chan: First-principles study on the electronic and optical properties of $BiFeO_3$. *Solid State Commun.* **149**, 641, 2009.
36. M. Veithen and PH. Ghosez: First-principles study of the dielectric and dynamical properties of lithium niobate. *Phys. Rev. B* **65**, 214302, 2002.
37. M. Nakayama, M. Nogami, M. Yoshida, T. Katsumata, and Y. Inaguma: First-principles studies on novel polar oxide $ZnSnO_3$: Pressure-induced phase transition and electric properties. *Adv. Mater.* **22**, 2579, 2010.
38. S. Baroni, S. de Gironcoli, A. Dal Corso, and P. Giannozzi: Phonons and related crystal properties from density functional perturbation theory. *Rev. Mod. Phys.* **73**, 515, 2001.
39. A. Roy, R. Prasad, S. Auluck, and A. Garg: First-principles calculations of born effective charges and spontaneous polarization of ferroelectric bismuth titanate. *J. Phys. Condens. Matter* **22**, 165902, 2010.
40. H. Wang, H.T. Huang, and B. Wang: First-principles study of structural, electronic, and optical properties of $ZnSnO_3$. *Solid State Commun.* **149**, 1849, 2009.
41. M. Xu, S.Y. Wang, G. Yin, J. Li, Y.X. Zheng, L.Y. Chen, and Y. Jia: Optical properties of cubic Ti_3N_4, Zr_3N_4 and Hf_3N_4. *Appl. Phys. Lett.* **89**, 151908, 2006.
42. Y. Syono, S. Akimoto, Y. Ishikawa, and Y. Endoh: A new high-pressure phase of $MnTiO_3$ and its magnetic property. *J. Phys. Chem. Solids* **30**, 1665, 1969.
43. X. Wu, S. Qin, and L. Dubrovinsky: Structural characterization of the $FeTiO_3$–$MnTiO_3$ solid solution. *J. Solid State Chem.* **183**, 2483, 2010.

Supplementary Material

Supplementary material can be viewed in this issue of the *Journal of Materials Research* by visiting http://journals.cambridge.org/jmr.